Least Square based Multi-spectral Color Interpolation Algorithm for RGB-NIR Image Sensors

Ji Yong Kwon, Chul Hee Park and Moon Gi Kang
Institute of BioMed-IT, Energy-IT and Smart-IT Technology (BEST), Yonsei University,
50 Yonsei-Ro, Seodaemun-Gu, Seoul, South Korea

Keywords: Color Interpolation, Demosaicking, Least Square, Near-Infrared, Multi-spectral Filter Array.

Abstract: The use of near-infrared (NIR) band gives us additional invisible information to discriminate objects and enables us to recognize objects more clearly under low light conditions. To acquire color and NIR bands together in a single image sensor developed from a conventional color filter array (CFA), we use a multi-spectral filter array (MSFA) in the RGB-NIR sensors and design a color interpolation algorithm to fill the information about the multi-spectral (MS) bands from the subsampled MSFA image. Aliasing in the MSFA image caused by the subsampled bands is minimized by balancing the energy of the bands. A panchromatic (PAN) image is generated by filtering the low-pass kernel to the MSFA image. This PAN image without chrominance signals, which contains the most high-frequency in the MSFA image, is used to reconstruct the MS images by solving the least square cost function between the PAN and MS images. The experiments show that the proposed algorithm estimates the high-resolution MS images very well.

1 INTRODUCTION

Security camera safety issues are increasing because many accidents and events take place abruptly. Especially at night, it is difficult to see and discriminate objects in dark areas. General digital cameras prevent a spectrum longer than 700 nm such as a near-infrared (NIR) band by using an infrared cutoff filter (IRCF) in front of the image sensors to preserve color information. However, a NIR band is invisible to the human eye and it provides additional information about objects in low light conditions. From these reasons, a NIR band is useful in fields such as vision, digital photography, and remote sensing (Zhang, 1999)(Schaul et al., 2009).

In the first study, to acquire three color bands together in one sensor, a conventional color filter array (CFA) was designed by the sub-sampled periodic patterns to reduce the cost and size of the sensors. To interpolate the missing color values, the method to reconstruct the color images with a frequency selective technique using luminance and chrominance was presented in (Alleysson et al., 2005). Based on an extension of the conventional CFA, to acquire several bands together, a multi-spectral filter array (MSFA) was described in (Lu et al., 2009). From this MSFA, the binary tree-based demosaicking method was proposed in (Miao et al., 2006). Also, multi-spectral demosaicking by upsampling using an adaptive kernel was introduced in (Monno et al., 2011). To reduce the demosaicking artifacts, vector based median filtering was presented in (Wang et al., 2013). To acquire color and NIR images using a single sensor, Zahara *et al.* designed a CFA pattern and demosaicing matrices in (Sadeghipoor et al., 2011). Also, a CFA that acquired color and a NIR image was designed by solving the spatial domain optimization problem in (Lu et al., 2009).

To acquire visible and invisible bands together, we use the RGB-NIR sensor presented in (Koyama et al., 2008). Theis sensor consist of four multi-spectral (MS) bands : red (R), green (G), blue (B), and NIR according to the MSFA pattern, as depicted in Fig. 1. Each four bands are sub-sampled within one quarter of the sensor. However, to acquire the NIR band in an image sensor, the IRCF has to be removed. This produces a color shift problem because color information as well as the NIR band is absorbed in the sensor. To solve this problem, a multi-layer decomposition method was explained in (Park et al., 2012).

In this paper, a least square based multi-spectral color interpolation algorithm for RGB-NIR sensors is presented. To minimize aliasing in the MSFA image, the energies of the MS bands are balanced.

Kwon J., Park C. and Kang M..
Least Square based Multi-spectral Color Interpolation Algorithm for RGB-NIR Image Sensors.
DOI: 10.5220/0005265000380045
In *Proceedings of the 10th International Conference on Computer Vision Theory and Applications* (VISAPP-2015), pages 38-45
ISBN: 978-989-758-089-5

Figure 1: The RGB-NIR sensor pattern.

A panchromatic (PAN) image without chrominance is generated from the MSFA image. The high-frequency of each MS image is retrieved using the high-frequency of the estimated PAN image with the least square minimization process. Experiments show that the proposed algorithm produces high quality results.

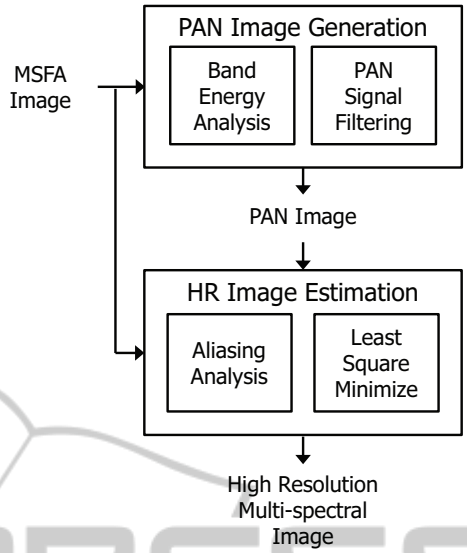

Figure 2: Overall block diagram of the proposed algorithm.

2 PROPOSED ALGORITHM

To obtain high-resolution R, G, B, and NIR images, we designed the algorithm as shown in Fig. 2. A two-step algorithm to reconstruct full resolution images is proposed. This paper is based on the assumption that the high-frequencies of the MS bands are highly correlated according to the spectral sensitivity described in (Koyama et al., 2008). First, the energies of the bands are balanced according to the band energy analysis process and the PAN image is obtained by filtering a low-pass kernel to the MSFA image. Second, the high-frequency of the MS bands is estimated using the high-frequency of the generated PAN image by finding the solution of the least square function.

2.1 Panchromatic Image Generation

Let $m[n_1,n_2]$ represent the MSFA image with size $N_1 \times N_2$, a pixel location of horizontal direction $n_1 = 0,\cdots,N_1-1$ and vertical direction $n_2 = 0,\cdots,N_2-1$, as the pattern illustrated in Fig. 1. Let R, G, B, and NIR bands be $m_b[n_1,n_2]$ where $b \in \{1,2,3,4\}$, respectively. The MSFA image is as follow,

$$\begin{aligned} m[n_1,n_2] &= \frac{1}{4}m_1[n_1,n_2](1+(-1)^{n_1})(1+(-1)^{n_2}) \\ &+\frac{1}{4}m_2[n_1,n_2](1-(-1)^{n_1})(1+(-1)^{n_2}) \\ &+\frac{1}{4}m_3[n_1,n_2](1+(-1)^{n_1})(1-(-1)^{n_2}) \\ &+\frac{1}{4}m_4[n_1,n_2](1-(-1)^{n_1})(1-(-1)^{n_2}). \end{aligned} \quad (1)$$

The four bands are acquired with sub-sampled in the MSFA image as,

$$\begin{aligned} m[n_1,n_2] &= \frac{1}{4}(m_1[n_1,n_2]+m_2[n_1,n_2] \\ &+m_3[n_1,n_2]+m_4[n_1,n_2]) \\ &+\frac{1}{4}(m_1[n_1,n_2]-m_2[n_1,n_2] \\ &-m_3[n_1,n_2]+m_4[n_1,n_2])(-1)^{n_1+n_2} \\ &+\frac{1}{4}(m_1[n_1,n_2]-m_2[n_1,n_2] \\ &+m_3[n_1,n_2]-m_4[n_1,n_2])(-1)^{n_1} \\ &+\frac{1}{4}(m_1[n_1,n_2]+m_2[n_1,n_2] \\ &-m_3[n_1,n_2]-m_4[n_1,n_2])(-1)^{n_2}. \end{aligned} \quad (2)$$

To see the Fourier spectrum of the MSFA image in the Fourier domain, the MSFA image is decomposed as a PAN signal m_P and three chrominance signals, m_{C_1}, m_{C_2}, and m_{C_3}. In terms of the signal decomposition to matrix notation, the relationship between the PAN signal and three chrominance signals, and the R, G, B, and NIR bands is,

$$\begin{pmatrix} m_P \\ m_{C_1} \\ m_{C_2} \\ m_{C_3} \end{pmatrix} = \frac{1}{4}\begin{pmatrix} 1 & 1 & 1 & 1 \\ 1 & -1 & -1 & 1 \\ 1 & -1 & 1 & -1 \\ 1 & 1 & -1 & -1 \end{pmatrix}\begin{pmatrix} m_1 \\ m_2 \\ m_3 \\ m_4 \end{pmatrix}. \quad (3)$$

Using the signal decomposition as (3), (1) is rewritten as

$$\begin{aligned} m[n_1,n_2] &= m_P[n_1,n_2]+m_{C_1}[n_1,n_2](-1)^{(n_1+n_2)} \\ &+m_{C_2}[n_1,n_2](-1)^{n_1}+m_{C_3}[n_1,n_2](-1)^{n_2}. \end{aligned} \quad (4)$$

Noting that $-1 = \exp(j\pi)$ and taking the Fourier transform to (4), the MSFA image is rewritten as

$$M(u,v) = M_P(u,v) + M_{C_1}(u-\pi, v-\pi) + M_{C_2}(u-\pi, v) + M_{C_3}(u, v-\pi). \quad (5)$$

This means that the Fourier spectrum of three chrominance signals $M_{C_1}(u,v)$, $M_{C_2}(u,v)$, and $M_{C_3}(u,v)$ are modulated at the frequencies (π,π), $(\pi,0)$, and $(0,\pi)$. According to the spectral sensitivity of the sensor in (Koyama et al., 2008), the NIR pixel is designed to absorb only the NIR band but the other color is also absorbed actually. In other words, all bands contain similar information. Also, basically, the color bands R, G, and B are highly correlated as mentioned in (Gunturk et al., 2002). Based on this, we suppose that the high-frequencies of the R, G, B, and NIR bands are highly correlated. Therefore, the aliasing invading the PAN signal from the chrominance signals is removed by balancing the energies of the bands because each chrominance signal is composed of two plus signals and two minus signals as discussed in (3).

We decompose the MS bands as low- and high-frequency as

$$M_b(u,v) = M_b^l(u,v) + M_b^h(u,v), \quad (6)$$

where $b \in \{1,2,3,4\}$. The mean values of the bands are calculated as

$$\mu_b = E(m_b[n_1,n_2]). \quad (7)$$

The maximum mean value μ_{max} is determined among the mean values of the four bands. Using this, the gain of each band is calculated according to the ratio between the maximum mean value and the mean value of each band as

$$g_b = \frac{\mu_{max}}{\mu_b}, \quad (8)$$

where $b \in \{1,2,3,4\}$. Applying the gains to each MS band, the modified bth MS band $M'_b[n_1,n_2]$ is computed as

$$M'_b(u,v) = g_b M_b(u,v), \quad (9)$$

where $b \in \{1,2,3,4\}$. The mean values of the bands are adjusted to a similar magnitude. This makes the high-frequency of the bands similar as

$$g_1 M_1^h(u,v) = g_2 M_2^h(u,v) = g_3 M_3^h(u,v) = g_4 M_4^h(u,v). \quad (10)$$

By using this process, the high-frequency of the chrominance signals are eliminated. That is to say, the chrominance signals invading the PAN signal are minimized.

$$\begin{aligned} M'_{C_1}(u,v) &= \frac{1}{4}M_1^{'l}(u,v) - \frac{1}{4}M_2^{'l}(u,v) - \frac{1}{4}M_3^{'l}(u,v) + \frac{1}{4}M_4^{'l}(u,v) \\ M'_{C_2}(u,v) &= \frac{1}{4}M_1^{'l}(u,v) - \frac{1}{4}M_2^{'l}(u,v) + \frac{1}{4}M_3^{'l}({}^l u,v) - \frac{1}{4}M_4^{'l}(u,v) \\ M'_{C_3}(u,v) &= \frac{1}{4}M_1^{'l}(u,v) + \frac{1}{4}M_2^{'l}(u,v) - \frac{1}{4}M_3^{'l}(u,v) - \frac{1}{4}M_4^{'l}(u,v). \end{aligned} \quad (11)$$

The three modified chrominance signals are obtained and the energy balanced MSFA signal $m'[n_1,n_2]$ is acquired as

$$m'[n_1,n_2] = m'_P[n_1,n_2] + m'_{C_1}[n_1,n_2](-1)^{(n_1+n_2)} + m'_{C_2}[n_1,n_2](-1)^{n_1} + m'_{C_3}[n_1,n_2](-1)^{n_2}. \quad (12)$$

With one PAN signal and three chrominance signals in the MSFA image overlapping, there is a trade-off between the signals when extracting one signal from the MSFA image. Therefore, we have to determine the adequate cutoff frequency of the low-pass kernel to acquire the PAN signal from the MSFA image. According to (Fang et al., 2012a), the majority of the spectrum energy of a typical signal is highly concentrated at a lower frequency, and the Laplacian probability density function is a good model to approximate the magnitude of the Fourier spectrum. Generally, the Fourier spectrums of the PAN and chrominance signals are approximated with the Laplacian model with each mean and variance. The cutoff frequencies are determined by matching two probability density functions between the Laplacian model of the PAN signal from $(0,0)$ and the Laplacian models of the chrominance signal from $(0,\pi)$, $(\pi,0)$, and (π,π). In other words, the cutoff frequency of the low-pass kernel $h_c[n_1,n_2]$ used to extract the PAN image can be determined. The process of conducting a convolution with a low-pass kernel $h_c[n_1,n_2]$ to the energy balanced MSFA signal $m'[n_1,n_2]$ can be written as

$$\hat{m}_P[n_1,n_2] = m'[n_1,n_2] * h_c[n_1,n_2]. \quad (13)$$

The PAN image is generated without chrominance signals containing the most high-frequency in the MSFA image, as illustrated in Fig. 3. The MSFA images are shown in Figs. 3(a) and (d). From this, the MSFA images with balanced energy are depicted in Figs. 3(b) and (e). By applying the low-pass kernel to the MSFA images with balanced energy in Figs. 3(b) and (e), the PAN images are generated as in Figs. 3(c) and (f).

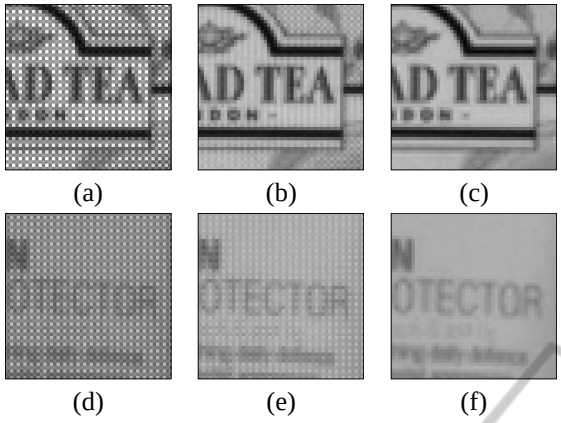

Figure 3: (a), (b), and (c) are parts of the *Sample1* image. (d), (e), and (f) are parts of the *Sample2* image. (a) and (d) MSFA pattern image. (b) and (e) Energy balanced MSFA pattern image. (c) and (f) Generated PAN image from (b) and (e), respectively.

2.2 HR Image Estimation

In this section, we estimate the high-resolution MS images by using the PAN image generated in the previous section. We denote the PAN image $m_P[n_1,n_2]$ and the MS images $m_b[n_1,n_2]$ by $\mathbf{P}$ and $\mathbf{M}_b$ in a $N\times 1$ lexicographical order where $N = N_1 \times N_2$, respectively. According to the formation of the synthetic PAN image (Zhang, 1999), the PAN images can be generated by a weighted sum with the coefficients of their MS images. The PAN image acquirement process can be represented as follows:

$$\mathbf{P} = \sum_{b=1}^{N_B} \alpha_b \mathbf{B}\mathbf{M}_b + \mathbf{w}, \tag{14}$$

where the blur matrix $\mathbf{B}$ is an assumed linear blur model and $\mathbf{w}$ refers to the Gaussian random noise. N_B represents the number of the spectral bands. The bth band coefficient of each band α_b according to the pixels is obtained through regression analysis using the relationship between the MS bands.

The low-frequency regions are important since they express the characteristics of the objects in the scene. Also, aliasing occurs mostly in high-frequency regions in the images. And we assume that each high-frequency of MS bands is highly correlated. For this reason, in this paper, we focused on the high-frequency reconstruction of the MS images. Therefore, the high-frequency of the MS images is estimated using the high-frequency of the PAN image. The PAN and MS images are decomposed into low- and high-frequency as

$$\begin{aligned} \mathbf{P} &= \mathbf{P}^l + \mathbf{P}^h, \\ \mathbf{M}_b &= \mathbf{M}_b^l + \mathbf{M}_b^h. \end{aligned} \tag{15}$$

Using the high-frequency signals only, (14) is rewritten as follows,

$$\mathbf{P}^h = \sum_{b=1}^{N_B} \alpha_b \mathbf{B}\mathbf{M}_b^h + \mathbf{w}. \tag{16}$$

The estimated bth band MS image is denoted by $\hat{\mathbf{M}}_b$. Also, the generated PAN image is denoted by $\hat{\mathbf{P}}$. Both the PAN image and the MS images from the MSFA image estimated in the previous section are used. In other words, the PAN image $\hat{\mathbf{P}}$ whose original expression is $\hat{m}_P[n_1,n_2]$ and the MS images from the energy balanced MSFA $m'[n_1,n_2]$ are used to estimate the high-resolution MS images. To minimize the difference between the high-frequency of the PAN image and those of the MS images, the least square problem is expressed as

$$\hat{\mathbf{M}}_b^h = \arg\min_{\mathbf{M}_b^h} ||\hat{\mathbf{P}}^h - \sum_{b=1}^{N_B} \alpha_b \mathbf{B}\mathbf{M}_b^h||^2. \tag{17}$$

Since the square error function (17) is convex, finding the minimization is equivalent to finding the zero value of its gradient. To find the minimization solution, the conjugate gradient descent method (Luenberger and Ye, 1984) is applied. Then, the high-frequency of the MS images is estimated in iterations as follows,

$$\hat{\mathbf{M}}_b^{h(n+1)} = \hat{\mathbf{M}}_b^{h(n)} + \varepsilon^{(n)}\{\mathbf{B}^\mathsf{T}(\hat{\mathbf{P}}^h - \alpha_b \mathbf{B}\hat{\mathbf{M}}_b^{h(n)})\}, \tag{18}$$

where ε and n refer to the iteration step and the iteration number, respectively. Estimating the MS bands in (18) refers to the fact that the high-frequency of the MS images are substituted by the that of the PAN image. The iteration ends when the relative difference energy $||\hat{\mathbf{P}}^h - \sum_{b=1}^{N_B} \alpha_b \mathbf{B}\hat{\mathbf{M}}_b^{h(n)}||^2$ between the high-frequency of the PAN image $\hat{\mathbf{P}}^h$ and those of the estimated MS band images with nth iteration $\hat{\mathbf{M}}_b^{h(n)}$ is smaller than the given threshold. The energy of high-frequency of the PAN image $||\hat{\mathbf{P}}^h||^2$ is used to normalize the relative difference energy. Finally, iteration ends when it satisfies the following condition,

$$\frac{||\hat{\mathbf{P}}^h - \sum_{b=1}^{N_B} \alpha_b \mathbf{B}\hat{\mathbf{M}}_b^{h(n)}||^2}{||\hat{\mathbf{P}}^h||^2} < T, \tag{19}$$

where T represents the specified threshold value. From (19), the high-frequency of the MS images are estimated. These images contain the high-frequency from the PAN image. As a result, the bth band high-resolution MS image is obtained as

$$\hat{\mathbf{M}}_b = \hat{\mathbf{M}}_b^h + \mathbf{M}_b^l. \tag{20}$$

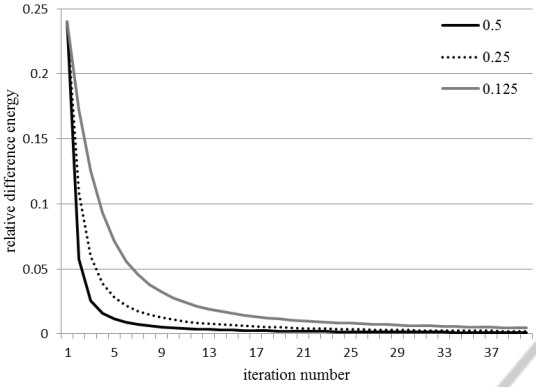

Figure 4: Rate of convergence for the *Sample3* image according to the step size.

The high resolution MS images are estimated by combining the low-frequency of the original MS images and the estimated high-frequency of the MS images. By estimating the high-frequencies of the MS images only, the high-frequency details of MS images are improved and the low-frequencies of the original MS images are preserved.

3 EXPERIMENTAL RESULTS

The results of the proposed algorithm are compared both objectively and subjectively with the results of the bilinear interpolation method and the BTES (Miao et al., 2006). First, the images acquired by the RGB-NIR sensors are used, *Sample1*, *Sample2*, *Sample3*, and *Sample4*, along with a resolution chart and objects with details. The R, G, B, and NIR bands of these images are sub-sampled by the MSFA pattern in Fig. 1. We tested the performance of the proposed algorithm by measuring the high-frequency energy (HFE) in (Fang et al., 2012b). Also, we obtained several original images using CCD sensors with changeable R, G, B, and NIR filters (*Sample5*, *Sample6*, *Sample7*, and *Sample8*) and measure the color-peak signal-to-noise ratio (CPSNR) of the resulting images. We generated the MSFA pattern image according to the pattern in Fig. 1 because each pixel contains the intensity values of the four bands (R, G, B, and NIR).

In the experiments, we assumed the variance of the blur kernel is 0.2 with a low blur condition and set the iteration step size ε at 0.5 in (18). The estimated MS images converged about 40 iterations when T is 10^{-3} in (19). The bth band coefficient α_b is $1/4$ equivalent for all bands. To decompose signals as low- and high-frequency, we use wavelet filters like the low-pass filter $[1,2,1]/4$ and the high-pass filter $[-1,2,-1]/4$. The initial value of the iterative estimation method is the results of the bilinear interpolation method.

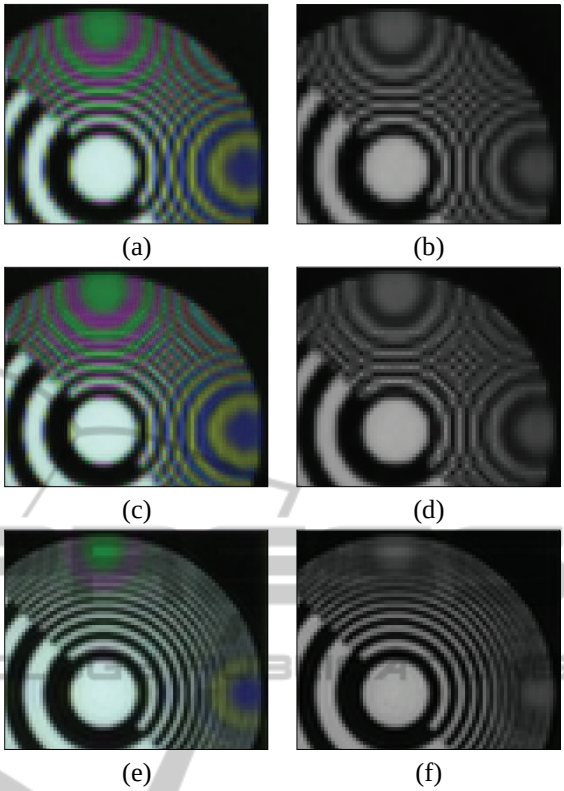

Figure 5: Part of the *Sample1* image. (a) Color result of the bilinear interpolation. (b) Color result of the BTES method. (c) Color result of the proposed algorithm. (d) NIR result of the bilinear interpolation. (e) NIR result of the BTES method. (f) NIR result of the proposed algorithm.

The rate of convergence to the minimized solution of the cost function is compared according to the iteration step sizes ε which are 0.5, 0.25, and 0.125. Fig. 4 describes the convergence of the iterations following the relative difference energy. The rate of convergence when ε is 0.5 is faster than that when ε are 0.25 and 0.125. From this, the proposed algorithm converges to find a solution.

3.1 Images Captured by RGB-NIR Sensors

The results of the proposed algorithm and other methods are shown for subjective image quality comparison. The results of the algorithms using the images captured by the RGB-NIR sensors are shown in Figs. 5-8. Figs. 5(a)-(d) and Figs. 6(a)-(d) show that the results obtained by the bilinear interpolation and the BTES methods contain aliasing artifacts such

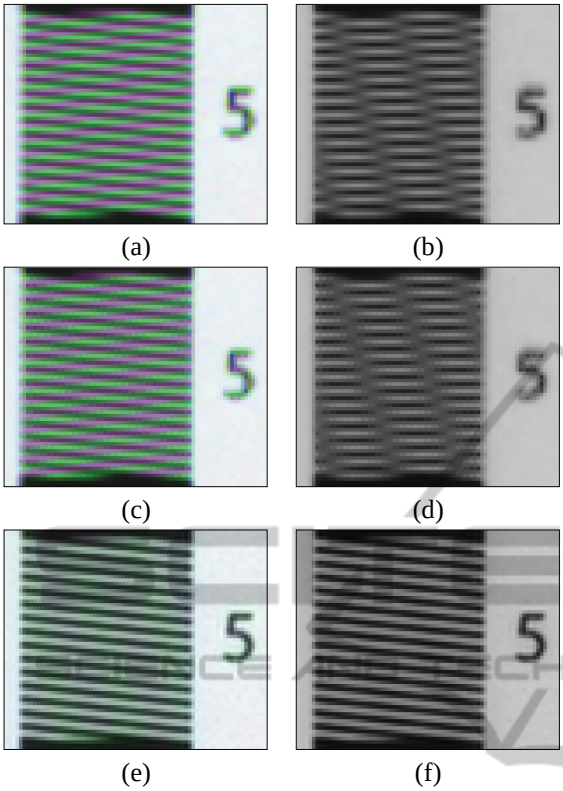

Figure 6: Part of the *Sample2* image. (a) Color result of the bilinear interpolation. (b) Color result of the BTES method. (c) Color result of the proposed algorithm. (d) NIR result of the bilinear interpolation. (e) NIR result of the BTES method. (f) NIR result of the proposed algorithm.

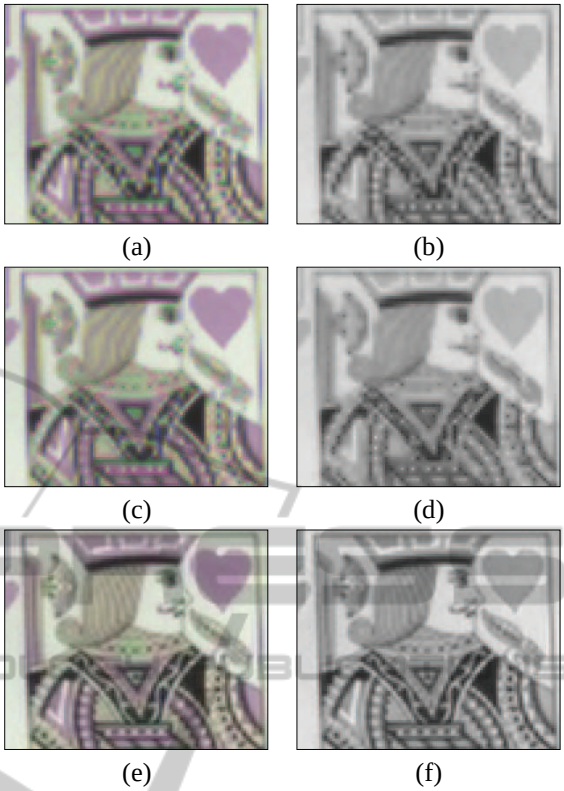

Figure 7: Part of the *Sample3* image. (a) Color result of the bilinear interpolation. (b) Color result of the BTES method. (c) Color result of the proposed algorithm. (d) NIR result of the bilinear interpolation. (e) NIR result of the BTES method. (f) NIR result of the proposed algorithm.

as false colors and zipper effects in the resulting images. However, the results of the proposed algorithm in Figs. 5(e) and (f) and Figs. 6(e) and (f) show that the image resolution improved greatly when using the proposed algorithm. In Figs. 7(a)-(d), the edges of the images are corrupted. However, Figs. 7(e) and (f) show that the proposed algorithm produces correct edges without any aliasing artifacts. While it is hard to recognize the letters in Figs. 8(a)-(d), Figs. 8(e) and (f) show the resulting edges to be well connected with clear letters. Finally, the amount of false colors and zipper effects in the high-frequency details decreased.

To objectively measure the improvement of the high-frequency details, the high-frequency energy (HFE) value is used in (Fang et al., 2012b). An image with a larger HFE is generally sharper. In this paper, this means that image resolution improved and the high-frequency details are reconstructed well. The image is convolved with two filters, h^k, with $k = 1, 2$. The two filters are high-pass filters $[1, -2, 1]$ applied in horizontal ($k = 1$) and vertical ($k = 2$) directions. Then, the HFE for the bth band image $m_b[n_1, n_2]$ is given by $\sum_{k=1}^{2} ||(h^k * m_b)[n_1, n_2]||_1/2$. The average HFE of the image is calculated as,

$$\mathrm{HFE}_b = \frac{\sum_{n_1=0}^{N_1-1} \sum_{n_2=0}^{N_2-1} \sum_{k=1}^{2} ||(h^k * m_b)[n_1, n_2]||_1/2}{N_1 N_2}. \quad (21)$$

We applied the HFE measurement to four images. Table 1 shows the HFE values of the resulting images for the four *Sample* images. The HFE values of the images produced by the proposed algorithm are higher than those of the other results. That is, the edges and high-frequency details of each image are reconstructed well.

3.2 Simulated Images

The results of the algorithms with the original image are illustrated in Fig. 9. We show the color images among the R, G, B, and NIR bands. Figs. 9(b) and (c) show that the edges are not connected well with

Figure 8: Part of the *Sample4* image. (a) Color result of the bilinear interpolation. (b) Color result of the BTES method. (c) Color result of the proposed algorithm. (d) NIR result of the bilinear interpolation. (e) NIR result of the BTES method. (f) NIR result of the proposed algorithm.

the false colors. However, by the proposed algorithm, the edges and high-frequency details in Fig. 9(d) are reconstructed well without leaving aliasing artifacts such as false colors.

To show a comparison of the objective image quality measurements, the CPSNR (in dB) is used as a performance measurement. We apply the CPSNR to four MS bands,

$$\text{CPSNR'} = 10\log_{10}\left(\frac{255^2}{\text{MSE}}\right), \tag{22}$$

where

$$\text{MSE} = \frac{\sum_{b=1}^{N_B}\sum_{n_1=0}^{N_1-1}\sum_{n_2=0}^{N_2-1}||m_b[n_1,n_2]-\hat{m}_b[n_1,n_2]||^2}{N_B N_1 N_2}. \tag{23}$$

Table 2 lists the CPSNR' values of the algorithms when applied to the four test images. In all instances, the proposed algorithm outperforms the other algorithms since high-frequency information is well reconstructed by the proposed least square method with the PAN image.

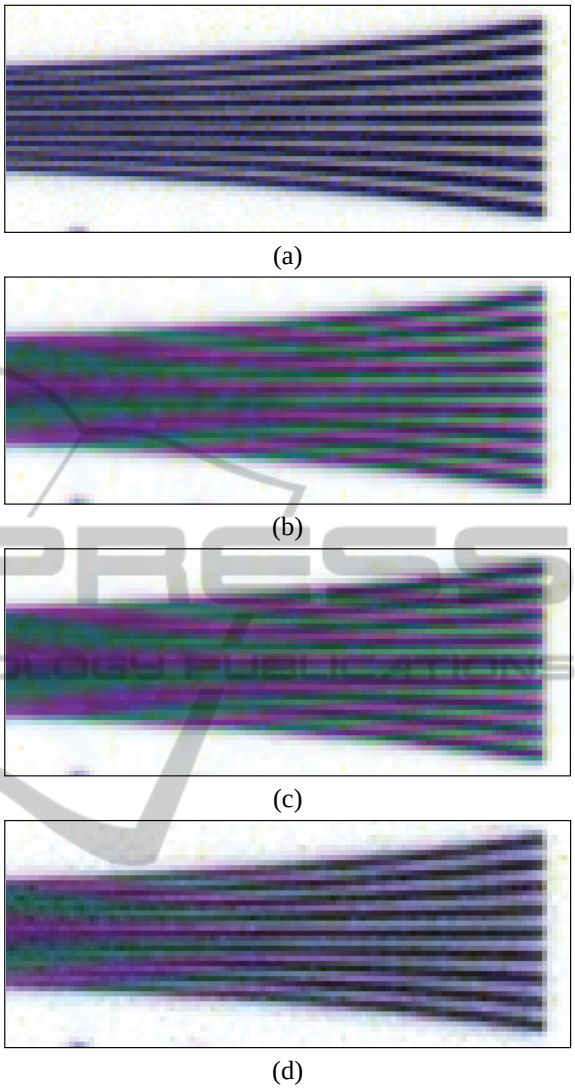

Figure 9: Part of the *Sample5* image. (a) Original image. (b) Result of the bilinear interpolation. (c) Result of the BTES method. (d) Result of the proposed algorithm.

4 CONCLUSIONS

In this paper, we presented a multi-spectral color interpolation algorithm for the RGB-NIR sensor that acquires invisible NIR band and visible color bands. This made objects clearer in dark conditions. The energies of the bands were compared and balanced similarly. From the balanced MSFA image, a PAN image was generated using a low-pass kernel with a high cutoff frequency. Our algorithm estimated the high-frequency of the MS images from the PAN image containing the high-frequency details without aliasing. The proposed algorithm can be adapted for any type

Table 1: HFE Performance Comparison For Four MSFA Images.

		Bilinear	BTES	Proposed
Sample1	R	5.76	6.77	**9.16**
	G	5.14	5.96	**9.14**
	B	4.07	4.65	**9.16**
	NIR	4.79	5.54	**9.14**
Sample2	R	3.06	3.46	**5.55**
	G	3.92	4.43	**5.56**
	B	2.45	2.69	**5.54**
	NIR	2.61	2.87	**5.54**
Sample3	R	7.54	8.99	**13.51**
	G	8.84	10.10	**13.61**
	B	8.26	9.63	**13.56**
	NIR	7.10	8.15	**13.45**
Sample4	R	9.24	10.64	**17.98**
	G	10.39	12.05	**17.99**
	B	9.95	11.51	**17.99**
	NIR	8.41	9.67	**17.97**

Table 2: CPSNR' (in decibels) Performance Comparison For Four Color Images.

	Bilinear	BTES	Proposed
Sample5	22.80	23.18	**24.16**
Sample6	22.93	23.12	**25.12**
Sample7	21.79	21.71	**24.44**
Sample8	21.84	21.38	**24.10**

of sub-sampled regular patterns because the method of reconstructing the high-frequency of the MS images is not related to any specific patterns.

ACKNOWLEDGEMENTS

This work was supported by the National Research Foundation of Korea (NRF) grant funded by the Korea government (MSIP) (No. 2012R1A2A4A01003732).

REFERENCES

Alleysson, D., Susstrunk, S., and Herault, J. (2005). Linear demosaicing inspired by the human visual system. *Image Processing, IEEE Transactions on*, 14(4):439–449.

Fang, L., Au, O., Tang, K., and Katsaggelos, A. (2012a). Antialiasing filter design for subpixel downsampling via frequency-domain analysis. *Image Processing, IEEE Transactions on*, 21(3):1391–1405.

Fang, L., Au, O., Tang, K., Wen, X., and Wang, H. (2012b). Novel 2-d mmse subpixel-based image down-sampling. *Circuits and Systems for Video Technology, IEEE Transactions on*, 22(5):740–753.

Gunturk, B., Altunbasak, Y., and Mersereau, R. (2002). Color plane interpolation using alternating projections. *Image Processing, IEEE Transactions on*, 11(9):997–1013.

Koyama, S., Inaba, Y., Kasano, M., and Murata, T. (2008). A day and night vision mos imager with robust photonic-crystal-based rgb-and-ir. *Electron Devices, IEEE Transactions on*, 55(3):754–759.

Lu, Y., Fredembach, C., Vetterli, M., and Susstrunk, S. (2009). Designing color filter arrays for the joint capture of visible and near-infrared images. In *Image Processing (ICIP), 2009 16th IEEE International Conference on*, pages 3797–3800.

Luenberger, D. G. and Ye, Y. (1984). *Linear and Nonlinear Programming*. Addison-Wesley.

Miao, L., Qi, H., Ramanath, R., and Snyder, W. (2006). Binary tree-based generic demosaicking algorithm for multispectral filter arrays. *Image Processing, IEEE Transactions on*, 15(11):3550–3558.

Monno, Y., Tanaka, M., and Okutomi, M. (2011). Multispectral demosaicking using adaptive kernel upsampling. In *Image Processing (ICIP), 2011 18th IEEE International Conference on*, pages 3157–3160.

Park, B. K., Choe, W., Lim, J., Lee, S., and Kim, C. (2012). Color correction with edge preserving and minimal snr decrease using multi-layer decomposition. volume 8296, pages 829613–829613–7.

Sadeghipoor, Z., Lu, Y., and Susstrunk, S. (2011). Correlation-based joint acquisition and demosaicing of visible and near-infrared images. In *Image Processing (ICIP), 2011 18th IEEE International Conference on*, pages 3165–3168.

Schaul, L., Fredembach, C., and Susstrunk, S. (2009). Color image dehazing using the near-infrared. In *Image Processing (ICIP), 2009 16th IEEE International Conference on*, pages 1629–1632.

Wang, X., Thomas, J.-B., Hardeberg, J. Y., and Gouton, P. (2013). Median filtering in multispectral filter array demosaicking.

Zhang, Y. (1999). A new merging method and its spectral and spatial effects. *International Journal of Remote Sensing*, 20(10):2003–2014.